Chinese Physics Letters

LETTER

Virtual State and Two-Pole Structure: (1690) and (1820) from BESIII data on (3686) +

Cite as: Jun He. 2026 *Chin. Phys. Lett.* **43** 090201

DOI CSTR

Recommended Articles

Experimental Advances on Light Baryon Spectroscopy at BESIII Experiment
Shi Wang, Hao Liu, Shuangshi Fang, and Xiongfei Wang
Chin. Phys. Lett. **43**, 050201 (2026)

Tests of CP Symmetry in Entangled Hyperon Antihyperon Pairs at BESIII
Wenjing Zheng, Andrzej Kupsc, Simone Pacetti, Francesco Rosini, Nora Salone, Xiongfei Wang, and Shuangshi Fang
Chin. Phys. Lett. **42**, 041201 (2025)

Prospects on Determining Electric Dipole Moments of Σand Ξ Hyperons at BESIII
ZHANG Feng, GAO Yuan-Ning, and HUO Lei
Chin. Phys. Lett. **27**, 051101 (2010)

Status and Prospect of Weak Radiative Hyperon Decays
Rui-Xiang Shi, Zekun Jia, Li-Sheng Geng, Haiping Peng, Qiang Zhao, and Xiaorong Zhou
Chin. Phys. Lett. **42**, 032401 (2025)

Search for the Low-Lying Excited Baryon $\Sigma^*(1/2^-)$ through Process $\Lambda_c+ \to \Lambda K^0 \pi^+$
Sheng-Chao Zhang, Wen-Tao Lyu, Guan-Ying Wang, Bo-Qiang Ma, and En Wang
Chin. Phys. Lett. **43**, 050203 (2026)

Non-Strange Baryon Spectra and Confinement in the Constituent Quark Model
LI Quan, PANG Hou-Rong, and PING Jia-Lun
Chin. Phys. Lett. **27**, 011201 (2010)

A series journal of Chinese Physical Society distributed by IOP Publishing

Chinese Physics Letters

Chin. Phys. Lett. 43 090201 (2026)

LETTER

DOI: 10.1088/0256-307X/43/9/090201
CSTR: 32039.14.0256-307X.43.9.090201

Virtual State and Two-Pole Structure: $\Xi(1690)$ and $\Xi(1820)$ from BESIII data on $\psi(3686) \to K^-\Lambda\bar{\Xi}^+$

Jun He*

School of Physics and Technology, Nanjing Normal University, Nanjing 210097, China

*Corresponding author. Email: junhe@njnu.edu.cn

We investigate the nature of the $\Xi(1690)$ and $\Xi(1820)$ resonances by analyzing the recent BESIII data on $\psi(3686) \to K^-\Lambda\bar{\Xi}^+$ within a coupled-channel rescattering framework. The calculation includes the channels $\bar{K}\Lambda$, $\bar{K}\Sigma^{(*)}$, $\pi\Xi^{(*)}$, $\eta\Xi^{(*)}$, and $K\Omega$. A direct fit to the data reveals that the $\Xi(1690)$ is best described as a virtual state located right below the $\bar{K}\Sigma$ threshold, a feature that naturally explains its very sharp peak observed in the $K^-\Lambda$ invariant mass spectrum. In contrast, the $\Xi(1820)$ exhibits a two-pole structure originating mainly from the coupled contributions of the $K\Sigma^*$ and $\pi\Xi^*$ channels, showing a two-pole pattern similar to that of the well-known $\Lambda(1405)$ and accounting for the unexpectedly broad width measured by BESIII. These findings provide new insights into the dynamical generation of hyperon resonances and highlight the importance of high-precision data from charmonium decays.

Introduction

In the past two decades, exotic hadrons have become a central theme, driven by observations in heavy-flavor sectors [1]. The idea, however, emerged earlier in the strange sector, e.g., the $\Lambda(1405)$ as a $\bar{K}N$ bound state [2–5] and the rise and fall of the pentaquark Θ [6], which later inspired the discovery of hidden-charm pentaquarks [7–10]. Recently, renewed attention has focused on hyperon resonances, including the $\Sigma^*(1/2^-)$ [11–13] and the $\Xi(1690)$ and $\Xi(1820)$, which are the subjects of this work. Early experiments established their existence and quantum numbers [14–18], but their nature remained unresolved. The new high-precision BESIII data on $\psi(3686) \to K^-\Lambda\bar{\Xi}^+$ [19,20] reveal two prominent peaks corresponding to $\Xi(1690)$ and $\Xi(1820)$ standing out from the background, providing a clean environment to address this question.

Constituent quark models predict the masses of $\Xi(1690)$ and $\Xi(1820)$ around 1750 MeV [21,22], significantly different from the PDG values [1]. Thus, they are natural candidates for dynamically generated states, as shown in the chiral unitary approach [23,24]. A model with vector meson-baryon channels explains the narrow width of $\Xi(1690)$ by its small couplings to decay channels [25], and a pole near the $\bar{K}\Sigma$ threshold emerges as a hadronic molecule state [26]. A recent work following the Belle measurement reproduces $\Xi(1690)$ with a next-to-leading order chiral interaction [27]. In the new BESIII measurement [20], the $\Xi(1690)$ peak lies just below the $\bar{K}\Sigma$ threshold and is very sharp, defying a standard Breit-Wigner description, a feature that has received little attention. This provides further evidence that $\Xi(1690)$ is a dynamically generated state rather than a conventional hyperon, a scenario we investigate here.

Likewise, the $\Xi(1820)$ also presents puzzles. The BESIII measurement shows a peak around $\Xi(1820)$ with an width of about 73 MeV [20], contrasting with the PDG average of 24 ± 5 MeV [1]. This large discrepancy has spurred theoretical work claiming the existence of two $\Xi(1820)$ states, as originally predicted within the chiral unitary approach [24]. In that framework, the interaction of pseudoscalar mesons with $J^P = 3/2^+$ decuplet baryons dynamically generates resonant states: a state around 1820 MeV and a wider pole in the 1800–1900 MeV region [24,28]. Motivated by the BESIII measurement, Ref. [29] revisited the $\Xi(1820)$ using coupled channels $\bar{K}\Sigma^*$, $\pi\Xi^*$, $\eta\Xi^*$, and ΩK, obtaining a good description with two poles at $1824 - 31i$ MeV and $1875 - 130i$ MeV. Subsequent work [30] proposed $\Xi_c \to \pi^+(\pi^0,\eta)\pi\Xi^*$ reactions, where interference between the two resonances leads to a dip around 1850 MeV in the $\pi(\eta)\Xi^*$ invariant mass distributions. The two-pole structure is an intriguing phenomenon in hadron spectroscopy, first demonstrated for $\Lambda(1405)$ and later found in other cases such as $D_0^*(2300)$ and $K_1(1270)$ [31–38]. These examples motivate our investigation into whether the $\Xi(1820)$ similarly arises from a two-pole scenario, which is the focus of this work.

Motivated by these considerations, we analyze the recent BESIII data on $\psi(3686) \to K^-\Lambda\bar{\Xi}^+$ to determine the nature of $\Xi(1690)$ and $\Xi(1820)$. Two features are key: (i) the $\Xi(1690)$ peak is very sharp and lies just below the $\bar{K}\Sigma$ threshold, defying a Breit–Wigner description and suggesting a dynamically generated state; (ii) the $\Xi(1820)$ exhibits an unexpectedly broad width, in sharp contrast to the PDG average, pointing to a possible two-pole structure. To address these issues, we employ a coupled-channel rescattering framework including $\bar{K}\Lambda$, $\bar{K}\Sigma^{(*)}$, $\pi\Xi^{(*)}$, $\eta\Xi^{(*)}$, and $K\Omega$, using the quasipotential Bethe–Salpeter equation (qBSE). Fitting the invariant mass spectra with the resulting amplitudes reveals the nature of these resonances. For reference, we also perform a conventional Breit–Wigner fit using effective Lagrangians.

Decay Mechanism

The BESIII data show two peaks, $\Xi(1690)$ and $\Xi(1820)$, in the $K^-\Lambda$ invariant mass spectrum, while no structures are seen in the $K^-\bar{\Xi}^+$ or $\Lambda\bar{\Xi}^+$ spectra. Two possible decay mechanisms are illustrated in Fig. 1.

Our main focus is the rescattering scenario [Fig. 1(a)], in which $\Xi(1690)$ and $\Xi(1820)$ arise as dynamically generated structures from coupled-channel interactions. Here, $\psi(3686)$ first decays into a meson-baryon pair, which then undergoes coupled-channel rescattering to produce the final $K^-\Lambda$ state. The included coupled channels are $\bar{K}\Lambda$, $\bar{K}\Sigma^{(*)}$, $\pi\Xi^{(*)}$, $\eta\Xi^{(*)}$, and $K\Omega$. For reference, we also consider the decay via intermediate Breit-Wigner resonances [Fig. 1(b)]. In that case, $\psi(3686)$ decays into a Ξ^* resonance accompanied by a $\bar{\Xi}^+$, followed by $\Xi^* \to K^-\Lambda$. This formalism, similar to that adopted in the experimental analysis, serves as a baseline for comparison.

Received 4 June 2026; accepted 4 August 2026; published 22 September 2026

© 2026 Chinese Physical Society and IOP Publishing Ltd. All rights, including for text and data mining, AI training, and similar technologies, are reserved.

Check for updates

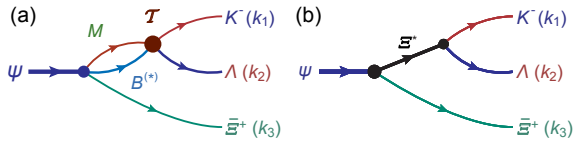

Fig. 1. Feynman diagrams for $\psi(3686) \to K^-\Lambda\bar{\Xi}^+$. Panel (a) shows the rescattering mechanism, where the brown filled circles represent the coupled-channel amplitudes $\mathcal{T}$. Panel (b) depicts the conventional Breit–Wigner mechanism with intermediate resonances.

The amplitudes of this Breit–Wigner formalism are derived from effective Lagrangians, with $\Xi(1690)$ and $\Xi(1820)$ treated as $1/2^-$ and $3/2^-$ resonances, respectively. The background is modeled as a wide Breit–Wigner resonance, either in the $K\Lambda$ channel with spin-parity $1/2^+$ or in the $\Lambda\bar{\Xi}^+$ channel with 0^-. The explicit Lagrangians, coupling constants, and propagators are provided in the Section S1 of Supplemental Material (SM). Following the experimental analysis [20], form factors are included to account for off-shell effects of the Ξ^* resonances.

Before calculating the total decay amplitude in the rescattering scenario [Fig. 1(a)], we first obtain the rescattering amplitudes for the coupled channels $\bar{K}\Lambda$, $\bar{K}\Sigma^{(*)}$, $\pi\Xi^{(*)}$, $\eta\Xi^{(*)}$, and $K\Omega$. For the interaction, we use the quasipotential Bethe–Salpeter equation (qBSE) combined with the one-boson-exchange model, where the potential is constructed from two vertices and a propagator. The vertices of pseudoscalar mesons $(\bar{K},\pi,\eta,K)$ and exchanged vector mesons (ρ,ω,ϕ,K^*) are described by the Lagrangian

$$\mathcal{L}_{\rm VPP} = -{\rm i}g\,{\rm Tr}\{V_\mu[P,\partial^\mu P]\}, \tag{1}$$

where the pseudoscalar and vector matrices are given by

$$P = \begin{pmatrix} \frac{1}{\sqrt{6}}\eta + \frac{1}{\sqrt{2}}\boldsymbol{\pi}\cdot\boldsymbol{\tau} & K \\ K^\dagger & -\frac{2}{\sqrt{6}}\eta \end{pmatrix},\ V = \begin{pmatrix} \frac{1}{\sqrt{2}}\omega + \frac{1}{\sqrt{2}}\boldsymbol{\rho}\cdot\boldsymbol{\tau} & K^* \\ K^{*\dagger} & \phi \end{pmatrix},$$

with $\boldsymbol{\tau}$ the Pauli matrices acting in isospin space. This form of the Lagrangian has been derived in many approaches, such as hidden local symmetry [39,40] and the direct SU(3) symmetry construction with $\alpha = 1$ [41,42]. The coupling constant is consistent across these formalisms and is given by $g = g_{\rho\pi\pi}/\sqrt{2}$, with $g_{\rho\pi\pi} \approx 6.1$ [39–45].

The vertices of baryons with exchanged vector mesons are described by the following Lagrangians. For the interactions of octet baryons B (Λ,Σ,Ξ) and decuplet baryons B^* (Σ^*,Ξ^*,Ω) with vector mesons V_ν, we have

$$\mathcal{L}_{BBV} = g_{NN\rho}\,\bar{B}\gamma^\nu V_\nu B, \tag{2}$$

$$\mathcal{L}_{B^*B^*V} = g_{\Delta\Delta\rho}\,\bar{B}^{*\mu}\gamma^\nu V_\nu B^*_\mu, \tag{3}$$

$$\mathcal{L}_{B^*BV} = -{\rm i}\frac{f_{\Delta N\rho}}{m_\rho}\,\bar{B}^{*\mu}\gamma^\nu\gamma^5 F_{\mu\nu} B, \tag{4}$$

where $F_{\mu\nu} = \partial_\mu V_\nu - \partial_\nu V_\mu$ is the field strength tensor. Here we neglect the tensor coupling, as in Ref. [46]; our calculation also confirms that its contribution is small, which facilitates a connection to the chiral unitary approach [4]. The coupling constants are taken as $g_{NN\rho} = g_{\rho\pi\pi}/2$ [42,43,45] and $g_{\Delta\Delta\rho} = g_{\rho\pi\pi}$ (close to the values in Ref. [42]), while the transition coupling is fitted to $f_{\Delta N\rho} = -6.08$ from Ref. [42]. The flavor structures of these vertices are provided in Section S2 of the SM.

Using the above Lagrangians, the vertices can be obtained, and the amplitudes for the potential kernel can be derived via standard Feynman rules. Following the method in Ref. [47], we directly implement the vertices Γ and propagators P into the code. The potential can be written using the Lagrangians and flavor wave functions as

$$\mathcal{V}_V = f_{\rm I}\,\Gamma_{1\mu}\Gamma_{2\nu}P_V^{\mu\nu}, \tag{5}$$

where $f_{\rm I}$ is the flavor factor, obtained from the flavor structures of the Lagrangians for mesons and baryons given above and the flavor wave functions (provided in Section S3 of the SM). The propagator is defined as $P_V^{\mu\nu} = {\rm i}(-g^{\mu\nu} + q^\mu q^\nu/m_V^2)/(q^2 - m_V^2)$ with $q = k - k'$ the four-momentum transfer and m_V the vector meson mass. For the specific channels considered in this work, the interaction potentials take relatively simple forms. We present the explicit expressions as follows,

$$\mathcal{V}_{MB\to MB} = C_{ij}g^2(k+k')_\mu\,\bar{u}\,\gamma_\nu u\,{\rm i}P_V^{\mu\nu}(q), \tag{6}$$

$$\mathcal{V}_{MB^*\to MB^*} = C_{ij}g^2(k+k')_\mu\,\bar{u}^\rho\,\gamma_\nu u_\rho\,{\rm i}P_V^{\mu\nu}(q), \tag{7}$$

$$\mathcal{V}_{MB\to MB^*} = C_{ij}g^2(k+k')_\mu\,\bar{u}^\rho(\gamma_\nu q_\rho - g_{\rho\nu}\not{q})u\,{\rm i}P_V^{\mu\nu}(q), \tag{8}$$

where C_{ij} are numerical coefficients that depend on the specific coupled channels. Their explicit values for $MB\to MB$ and $MB^*\to MB^*$ are provided in Section S3 of the SM. In the above, u $(\bar{u})$ denote the Dirac spinors of initial (final) octet baryons, while u_ρ $(\bar{u}^\rho)$ are the Rarita–Schwinger spinors for decuplet baryons. In the limit $q^2 \ll m_V^2$, neglecting the $q^\mu q^\nu$ term, the potential reduces to a contact interaction and coincides with that used in the chiral unitary approach [23,24].

The rescattering amplitude $\mathcal{T}$ [Fig. 1(a)] is obtained by inserting the potential kernel $\mathcal{V}$ through the Bethe-Salpeter equation. Using the quasipotential approximation and partial-wave decomposition, the four-dimensional integral reduces to a one-dimensional integral equation for each $J^{\rm P}$,

$$\begin{aligned}{\rm i}\mathcal{T}^{J^{\rm P}}_{\lambda_1,\lambda_2;\lambda_1',\lambda_2'}(p',p) = {\rm i}\mathcal{V}^{J^{\rm P}}_{\lambda_1,\lambda_2;\lambda_1',\lambda_2'}(p',p) + \frac{1}{2}\sum_{\lambda_1'',\lambda_2''}\int\frac{p''^2{\rm d}p''}{(2\pi)^3}\\ \cdot{\rm i}\mathcal{V}^{J^{\rm P}}_{\lambda_1,\lambda_2;\lambda_1'',\lambda_2''}(p',p'')G_0(p''){\rm i}\mathcal{T}^{J^{\rm P}}_{\lambda_1'',\lambda_2'';\lambda_1',\lambda_2'}(p'',p).\end{aligned} \tag{9}$$

The explicit can be found in our previous works [48–52], and Section S4 in the SM. An exponential regulator $G_0(p'') \to G_0(p'')e^{-2(p_i''^2 - m_i^2)^2/\Lambda^4}$ is introduced [49].

The decay amplitude is also partial-wave decomposed including parity [13],

$$\begin{aligned}{\rm i}\mathcal{M}_{\lambda_1,\lambda_2,\lambda_3;\lambda}(p_1,p_2,p_3) = \sum_{J^{\rm P}M}\frac{2J+1}{4\pi}D^{J*}_{M\lambda_{21}}(\Omega_2)\int\frac{p'^2{\rm d}p'}{(2\pi)^3}\cdot\\ \sum_{\lambda_1',\lambda_2'}{\rm i}\mathcal{T}^{J^{\rm P}}_{\lambda_1,\lambda_2;\lambda_1',\lambda_2'}(p_j',s_{12})\,G_0(p')\cdot\\ {\rm i}\mathcal{A}^{J^{\rm P}M}_{\lambda_1',\lambda_2';\lambda_3;\lambda}(p_j',\Omega_3,s_{12}),\end{aligned} \tag{10}$$

where Ω_2, Ω_3 are solid angles of $\Lambda, \bar{\Xi}^+$, s_{12} is the $K^-\Lambda$ invariant mass, and $D^{J*}_{M\lambda_{21}}$ is a Wigner D-function. The amplitude $\mathcal{A}$ is described by the effective Lagrangians

$$\mathcal{L}_{\psi\to MB^*\bar{\Xi}^+} = g_{B^*M}\,\bar{B}_\mu M\gamma_\nu\psi^\mu\partial^\nu\bar{\Xi}^+, \tag{11}$$

$$\mathcal{L}_{\psi\to MB\bar{\Xi}^+} = g_{BM}\,\bar{B}M\psi_\mu\partial^\mu\bar{\Xi}^+. \tag{12}$$

It should be noted that we consider the decay $\psi(3686)\to K^-\Lambda\bar{\Xi}^+$, and the rescattering occurs in the $K^-\Lambda$ channel, which has total isospin $I = 1/2$. In principle, the intermediate states should include all coupled channels: $MB^{(*)} = \bar{K}\Lambda$, $\bar{K}\Sigma^{(*)}$, $\pi\Xi^{(*)}$, $\eta\Xi^{(*)}$, and $K\Omega$, with isospin $I = 1/2$. As shown in Ref. [53], $\psi(3686)$, being a $c\bar{c}$ state, is an SU(3) singlet (for u,d,s quarks). Consequently, the decay amplitudes to the MB channels are related within that sector, and likewise for the MB^* channels, but there is no relation between the two sectors. The fit results show that the contributions from the MB channels are numerically very small, while the MB^* channels play an essential role in generating the near-threshold structures observed in the data. We therefore retain only the MB^* channels as intermediate channels. Their relative contributions for $I = 1/2$ states, based on SU(3) symmetry, are $\bar{K}\Sigma^* : \pi\Xi^* : \eta\Xi^* : K\Omega = 1 : -1 : -1 : \sqrt{2}$ [41,53]. For the rescattering mechanism, the form factors adopted in the BESIII analysis [20] centered at the resonance pole masses m_{Ξ^*} are not suitable. Therefore, we introduce a different form factor at the decay vertices, based on the $K\Lambda$ threshold: $F(s_{12}) = \Lambda^4/(\Lambda^4 + (s_{12} - m_{\rm thr}^2)^2)$ where

Table 1. Fit parameters and χ^2 values for different scenarios: BW (Breit–Wigner) and RS (rescattering). Backgrounds (bk) are added in either $K^-\Lambda$ or $\Lambda\bar{\Xi}^+$ spectra, as indicated. Strength parameters g are in relative units (only magnitudes meaningful), phases ϕ dimensionless, masses m and widths Γ in MeV. Fit quality: $\chi^2_{\rm tot}$/ndf (total chi-squared per degree of freedom).

Fits	BW($K^-\Lambda$)	BW($\Lambda\bar{\Xi}^+$)	RS($K^-\Lambda$)	RS($\Lambda\bar{\Xi}^+$)
$g_{\Xi(1690)}$	$0.247^{+0.004}_{-0.004}$	$0.194^{+0.004}_{-0.003}$	$35.33^{+0.46}_{-0.33}$	$32.51^{+0.26}_{-0.75}$
$\phi_{\Xi(1690)}$	$1.948^{+0.004}_{-0.003}$	$0.282^{+0.002}_{-0.003}$	$0.338^{+0.199}_{-0.037}$	$0.822^{+0.134}_{-0.056}$
$m_{\Xi(1690)}$	$1682.9^{+3.0}_{-4.8}$	$1667.3^{+2.1}_{-5.5}$	–	–
$\Gamma_{\Xi(1690)}$	$134.8^{+3.2}_{-2.8}$	$92.0^{+2.0}_{-2.3}$	–	–
$g_{\Xi(1820)}$	$4.834^{+0.093}_{-0.056}$	$4.686^{+0.088}_{-0.070}$	$65.16^{+1.60}_{-1.20}$	$62.94^{+0.67}_{-2.98}$
$\phi_{\Xi(1820)}$	$1.165^{+0.031}_{-0.025}$	$1.010^{+0.031}_{-0.001}$	$1.062^{+0.238}_{-0.323}$	$0.565^{+0.028}_{-0.191}$
$m_{\Xi(1820)}$	$1820.8^{+1.9}_{-1.9}$	$1821.2^{+2.0}_{-2.6}$	–	–
$\Gamma_{\Xi(1820)}$	$94.0^{+2.0}_{-2.2}$	$100.0^{+2.8}_{-2.2}$	–	–
$g_{\rm bk}$	$1.054^{+0.023}_{-0.020}$	$9.128^{+0.212}_{-0.122}$	$0.603^{+0.039}_{-0.034}$	$11.39^{+0.16}_{-0.54}$
$m_{\rm bk}$	$2034.9^{+9.4}_{-8.9}$	$2846.0^{+6.3}_{-5.6}$	$1911.4^{+32.6}_{-32.7}$	$2885.4^{+5.6}_{-6.0}$
$\Gamma_{\rm bk}$	$1489.3^{+29.0}_{-32.8}$	$860.1^{+12.5}_{-19.8}$	$1394.4^{+89.5}_{-82.4}$	$1106.1^{+56.1}_{-16.9}$
$\chi^2_{\rm tot}$/ndf	1.7059	2.0103	2.4127	1.6671

$m_{\rm thr} = m_K + m_\Lambda$ is the $K\Lambda$ threshold mass, and cutoff $\Lambda = 1$ GeV.

The partial-wave vertex $\mathcal{A}^{JPM}$ is obtained from the amplitudes $\mathcal{A}$ via a partial-wave decomposition:

$$\mathcal{A}^{JPM}_{\lambda_1',\lambda_2';\lambda_3;\lambda} = \int \mathrm{d}\Omega_2' [D^J_{M,\lambda_{21}'}(\Omega_2')\mathcal{A}_{\lambda_1',\lambda_2';\lambda_3;\lambda} + \eta' D^J_{M,-\lambda_{21}'}(\Omega_2')\mathcal{A}_{-\lambda_1',-\lambda_2';\lambda_3;\lambda}(\Omega_2')], \quad (13)$$

where $\lambda_{21}' = \lambda_2' - \lambda_1'$ is the helicity difference of the two intermediate particles, and $\eta' = PP_1P_2(-1)^{J-J_1-J_2}$ is the parity factor, with P the intrinsic parity of the system, P_1, P_2 the parities of the two constituents, and J, J_1, J_2 the total and individual spins.

The experimental analysis suggests that the data can be described by two resonances plus a background contribution. Following the experimental procedure, the total decay amplitude is expressed as

$$\mathcal{M} = \mathrm{e}^{\mathrm{i}\pi\phi_{\Xi(1690)}}\mathcal{M}_{\Xi(1690)} + \mathrm{e}^{\mathrm{i}\pi\phi_{\Xi(1820)}}\mathcal{M}_{\Xi(1820)} + \mathcal{M}_{\rm bk}, \quad (14)$$

where $\mathrm{e}^{\mathrm{i}\pi\phi_{\Xi^*}}$ and $\mathcal{M}_{\Xi^*}$ denote the relative phase and amplitude associated with the resonance Ξ^*, each of which will be described either by Breit–Wigner intermediate states or by rescattering effects. The background contribution is modeled as a wide Breit–Wigner resonance in two scenarios, following the experimental analysis [20].

With the decay amplitude, the differential decay width is given by

$$\mathrm{d}\Gamma = \frac{1}{2M_\psi}\sum|\mathcal{M}|^2\mathrm{d}\Phi, \quad (15)$$

where M_ψ is the mass of the initial $\psi(3686)$ meson, and $\mathrm{d}\Phi$ denotes the Lorentz-invariant phase space element. In this work, the phase space element $\mathrm{d}\Phi$ is simulated using the method proposed in Ref. [54], implemented in the Julia programming language. The corresponding Julia package `DalitzPlot.jl`, which simulates decays based on our qBSE approach, is available on GitHub [55]. A total of 10^7 events are generated. The momenta of the final-state particles are sampled via a Monte Carlo approach that strictly enforces energy-momentum conservation. From these simulated momenta, the invariant mass spectra are constructed and subsequently used in the analysis.

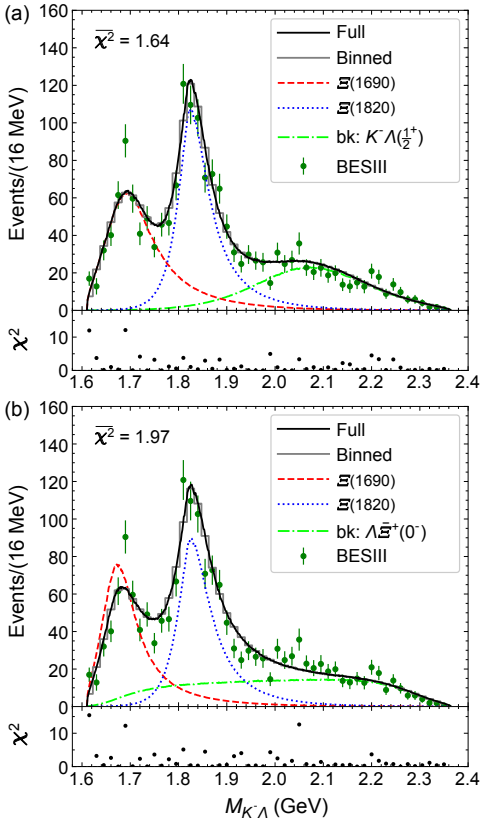

Fig. 2. $K^-\Lambda$ invariant mass spectra in the Breit–Wigner scenario. The curves correspond to the full model (solid black), $\Xi(1690)$ (red dashed), $\Xi(1820)$ (blue dotted), and background (green dash-dotted). The binned results are also shown as a gray histogram. The data are taken from the BESIII Collaboration [20]. The scatter points in the lower part of each panel represent the individual χ^2 contributions of the corresponding data points. Panel (a) shows the fit with a background in $K^-\Lambda$ ($1/2^+$), and panel (b) shows the fit with a background in $\Lambda\bar{\Xi}^+$ (0^-).

Numerical Results

We first fit the BESIII invariant mass spectra of $K^-\Lambda$, $K^-\bar{\Xi}^+$, and $\Lambda\bar{\Xi}^+$ using Breit–Wigner resonances $\Xi(1690)$ and $\Xi(1820)$, with the background as a wide Breit–Wigner resonance in $K^-\Lambda$ or $\Lambda\bar{\Xi}^+$ (second and third columns of Table 1). This fit has 11 parameters (strength, phase, mass, width for each Ξ^*, plus three background parameters). The $\chi^2 = \sum_{i=1}^{N_{\rm bin}}(n_i - \nu_i)^2/\nu_i$ follows the experimental definition [20]. The strength parameters, $g_{\Xi(1690)}$, $g_{\Xi(1820)}$, and $g_{\rm bk}$, absorb coupling constants and are scaled to the overall yield; only their relative values matter. We use the Julia package `optimize.jl` for the fit. With a background in $K^-\Lambda$, we obtain $\chi^2_{\rm tot}$/ndf = 1.7059, close to the experimental result, while a background in $\Lambda\bar{\Xi}^+$ gives $\chi^2_{\rm tot}$/ndf = 2.0103. Our main focus, however, is the rescattering scenario (fourth and fifth columns of Table 1), where the $\Xi(1690)$ and $\Xi(1820)$ are dynamically generated; only strength and phase parameters are fitted there. Remarkably, with the background in $\Lambda\bar{\Xi}^+$, the rescattering

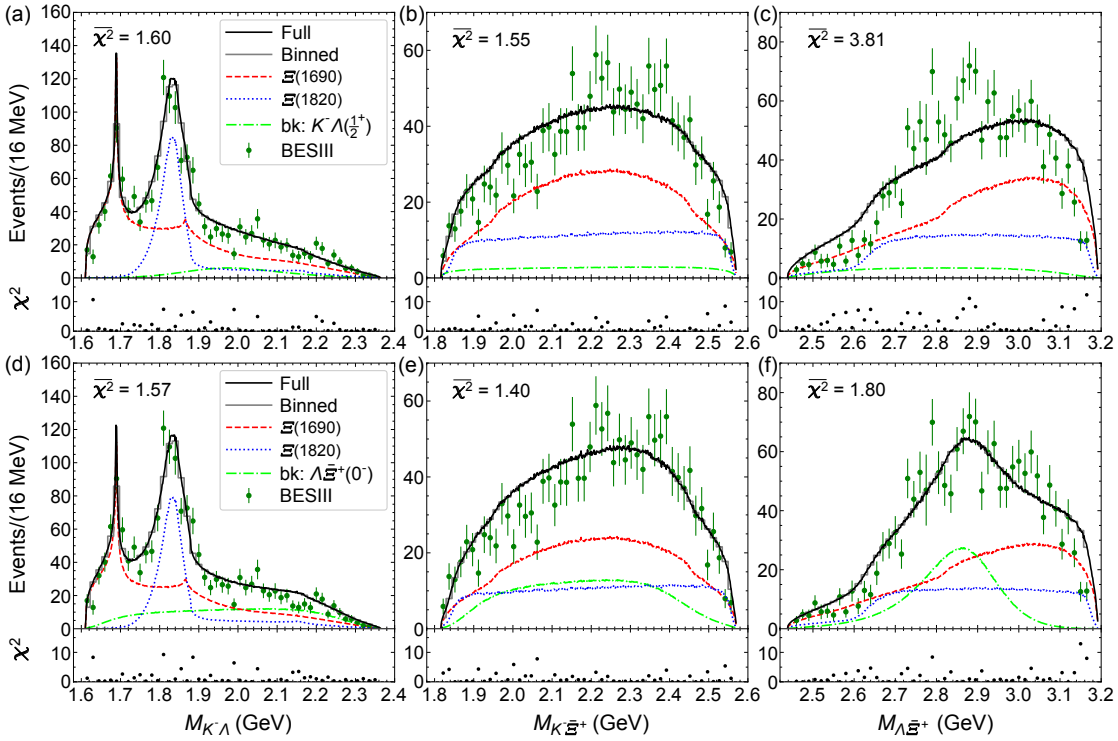

Fig. 3. Invariant mass spectra in the rescattering scenario. Panels (a)–(c) correspond to the fit with a background in $K^-\Lambda$ $(1/2^+)$, and panels (d)–(f) to the fit with a background in $\Lambda\bar{\Xi}^+$ (0^-). Other notations are the same as in Fig. 2.

scenario yields $\chi^2_{\rm tot}/{\rm ndf} = 1.6671$, an excellent fit that demonstrates its ability to describe the data.

The results for the Breit-Wigner scenario are illustrated in Fig. 2 (the full set of results for the three invariant mass spectra of $K^-\Lambda$, $K^-\bar{\Xi}^+$, and $\Lambda\bar{\Xi}^+$ is provided in Section S5 of the SM). Our treatment is similar to that adopted in the experimental analysis, but with effective Lagrangians. The fit includes three components: two Breit–Wigner resonances for $\Xi(1690)$ and $\Xi(1820)$, and one for the background.

As in the experimental analysis, the $K^-\Lambda$ invariant mass spectrum can be well reproduced with two Ξ^* states and a background in $K^-\Lambda$ with $1/2^+$. The average χ^2 values for the $K^-\Lambda$, $K^-\bar{\Xi}^+$, and $\Lambda\bar{\Xi}^+$ spectra obtained from this fit are 1.64, 1.12, and 2.06, respectively (see Fig. 2(a) for $K^-\Lambda$; the $K^-\bar{\Xi}^+$ and $\Lambda\bar{\Xi}^+$ spectra are shown in the SM). These values are close to those reported by the BESIII collaboration (1.46, 1.10, and 2.16) [20]. As shown in Fig. 2(a), the peaks around 1700 and 1800 MeV in the $K^-\Lambda$ spectrum clearly originate from the two Breit–Wigner resonances, while the background mainly contributes to the higher energy region. Replacing the background in $K^-\Lambda$ with one in $\Lambda\bar{\Xi}^+$ (0^-) yields a slightly improved χ^2 for the $\Lambda\bar{\Xi}^+$ spectrum (from 2.06 to 1.89) but worsens the fits for $K^-\Lambda$ and $K^-\bar{\Xi}^+$ (χ^2 values increase to 1.97 and 1.72, respectively), consistent with the experimental finding that the background in $K^-\Lambda$ with $1/2^+$ is the best choice [20].

An important observation is that the experimental peak around 1700 MeV is very sharp. Neither of the fits shown in Figs. 2(a) and 2(b) can reproduce such a sharp peak; in fact, even the original experimental analysis using Breit–Wigner resonances failed to describe it [20]. This provides strong evidence that the peak does not originate from a conventional Breit–Wigner resonance, but rather points to a non-resonant or dynamically generated nature.

Now we replace the Breit–Wigner resonances with the rescattering mechanism. Specifically, we consider coupled-channel interactions involving $\bar{K}\Lambda$, $\bar{K}\Sigma^{(*)}$, $\pi\Xi^{(*)}$, $\eta\Xi^{(*)}$, and $K\Omega$. The lower peak, $\Xi(1690)$, originates mainly from the interaction of octet baryons with pseudoscalar mesons, i.e., $\bar{K}\Lambda$, $\bar{K}\Sigma$, $\pi\Xi$, and $\eta\Xi$, in an S-wave, which forms a system with $J^{\rm P} = 1/2^-$, consistent with the experimental suggestion. The higher peak, $\Xi(1820)$, arises primarily from the channels $\bar{K}\Sigma^*$, $\pi\Xi^*$, and $\eta\Xi^*$ in an S-wave, which forms a system with $J^{\rm P} = 3/2^-$, also consistent with the experimental suggestion. In the calculation, the couplings among all these channels are fully considered. We find that with a cutoff $\Lambda = 1.15$ GeV, a peak near 1800 MeV is generated, as shown in Figs. 3(a) and 3(d).

Unlike the $\Xi(1820)$, which can be reproduced by both a Breit-Wigner resonance and the rescattering mechanism, the $\Xi(1690)$ cannot be well fitted by a Breit-Wigner resonance, as shown in Fig. 2 and in the original experimental analysis. The main issue is that the experimental peak is too sharp and does not follow a standard Breit–Wigner shape. Such a sharp peak is a natural feature of a molecular state near threshold, and can be well described by our rescattering mechanism. While a Flatté-like parametrization can also produce a similar sharp peak near threshold, it remains purely phenomenological and does not provide access to the underlying dynamics, which are naturally obtained in our qBSE approach. To find the best description of the data, we adjust the cutoff for the $\bar{K}\Sigma$ channel and set it to 0.5 GeV. As shown in Figs. 3(a) and 3(d), a very sharp peak is reproduced from the coupled-channel rescattering. The maximum value of the peak is slightly higher than the experimental data points, which is due to the binning of the data at intervals of 16 MeV. After binning the theoretical results (gray histogram in Fig. 3), the binned results are found to fit the data well.

The rescattering amplitudes with spin parity $1/2^-$ and $3/2^-$ can reproduce the two peaks around 1700 and 1800 MeV. Unlike the fit with Breit–Wigner resonances, the $1/2^-$ contribution appears in almost the entire energy region of the $K^-\Lambda$ invariant mass spectrum. Besides providing the $\Xi(1690)$ peak, a clear effect of this contribution is also seen in the $\Xi(1820)$ peak, and it becomes even more important in the other two invariant mass spectra. If we choose the background in the $K^-\Lambda$ channel, the background contribution is suppressed due to the $1/2^-$ rescattering contribution. However, with such a small background, the $\Lambda\bar{\Xi}^+$ invariant mass spectrum cannot be well reproduced, yielding an average χ^2 of about 3.81. To improve the fit in all three invariant mass spectra, we move the background to the $\Lambda\bar{\Xi}^+$ channel. An excellent fit is then achieved with two rescattering contributions ($1/2^-$ and $3/2^-$) and a $\Lambda\bar{\Xi}^+(0^-)$ background. The

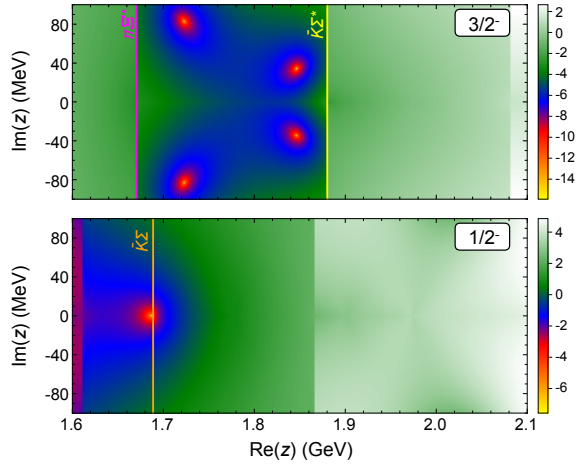

Fig. 4. Poles with spin-parities $3/2^-$ (upper panel) and $1/2^-$ (lower panel) from the coupled-channel interactions. The colorbox represents $\log|1-V(z)G(z)|$. Vertical dashed lines mark the positions of the $\bar{K}\Sigma^*$, $\pi\Xi^*$ (upper panel) and $\bar{K}\Sigma$ (lower panel) thresholds.

average χ^2 values for $K^-\Lambda$, $K^-\bar{\Xi}^+$, and $\Lambda\bar{\Xi}^+$ become 1.57, 1.40, and 1.80, respectively, with a total reduced χ^2 of 1.667, which is very close to the experimental values.

In the above, with rescatterings in the $K^-\Lambda$ channel, the experimental data can be well reproduced. The coupled-channel interactions including $\bar{K}\Lambda$, $\bar{K}\Sigma^{(*)}$, $\pi\Xi^{(*)}$, $\eta\Xi^{(*)}$, and $K\Omega$ reproduce the correct invariant mass spectra. Now, we provide the poles of these coupled-channel interactions in the complex energy plane, as shown in Fig. 4, to discuss the nature of the $\Xi(1690)$ and $\Xi(1820)$.

To locate the poles, we adopt the method of Ref. [35]. For each two-body channel, we choose the first (physical) Riemann sheet below its threshold and the second (unphysical) sheet above threshold; this convention ensures that the resulting pole positions and half-widths can be meaningfully compared to Breit-Wigner parameters extracted from the real axis. In the $3/2^-$ partial wave (upper panel of Fig. 4), two poles are clearly visible. The pole near $1846-34i$ MeV lies close to the $K\Sigma^*$ threshold (approximately 1880 MeV). A single-channel analysis reveals that this pole originates from a bound state of the $K\Sigma^*$ interaction; when coupled channels are switched on, the bound state acquires an imaginary part because it can decay into other channels (e.g., $\pi\Xi^*$), thereby turning into a resonance with a finite width. The second pole at $1724-80i$ MeV is located above the $\pi\Xi^*$ threshold. Since it is a resonance mainly generated by the $\pi\Xi^*$ interaction, it carries an imaginary part already in the single-channel calculation, and this width is further enlarged by coupled-channel effects; hence, it naturally has a larger width. One can also note that the real part of the higher pole (1846 MeV) is higher than the Breit–Wigner mass and those reported in Ref. [30], and the existence of the lower pole shifts the peak slightly lower relative to the experimental one. The co-existence of these two poles in the same J^P partial wave constitutes a two-pole structure, which underlies the observed line shape in the $K^-\Lambda$ invariant mass spectrum: the higher pole dominates the peak near 1820 MeV, while the lower pole contributes with a broader width.

In the $1/2^-$ partial wave (lower panel), only one pole is found near 1690 MeV, which is essential for reproducing the very sharp peak in the data. This pole lies almost exactly at the $K\Sigma$ threshold. A detailed analysis of its location in the complex plane reveals that it is not a state on the physical sheet but a virtual state: it resides on the second Riemann sheet of the $K\Sigma$ channel at 1687.1 MeV, approximately 1.7 MeV below the $K\Sigma$ threshold. Virtual states are characterized by a pole on the real axis just below threshold on the unphysical sheet, producing a cusp-like enhancement in the scattering amplitude rather than a typical Breit–Wigner peak. To visualize this pole, in the lower panel we specifically choose the second Riemann sheet for the $K\Sigma$ channel, while for the other channels we adopt the same prescription as used in the $3/2^-$ case. A clear virtual state then appears as a localized structure below the $K\Sigma$ threshold. This virtual state is a direct consequence of the attractive $\bar{K}\Sigma$ interaction in the S-wave, which is too weak to form a bound state but sufficiently strong to produce a near-threshold singularity. This virtual state is robust against variations of the cutoff parameter, as discussed in Section S6 of the SM. This stability, together with the fact that the data strongly favor this scenario over bound-state interpretation, supports the virtual-state nature of the $\Xi(1690)$.

Summary

The Breit–Wigner fits, similar to the experimental analysis, reproduce the overall spectra reasonably well but fail to describe the very sharp $\Xi(1690)$ peak near the $\bar{K}\Sigma$ threshold. In contrast, the rescattering mechanism naturally produces this sharp peak, which arises from a virtual state located about 1.7 MeV below the threshold in the $1/2^-$ partial wave. The current BESIII data thus support the interpretation that $\Xi(1690)$ is not a conventional three-quark state but a dynamically generated virtual state from $\bar{K}\Sigma$ interactions. Future high-precision data will be essential to further test this scenario.

For $\Xi(1820)$, the rescattering calculation yields a two-pole structure in the $3/2^-$ partial wave: a pole at $1846-34i$ MeV below the $K\Sigma^*$ threshold (originating from a bound state) and another at $1724-80i$ MeV above the $\pi\Xi^*$ threshold (originating from a resonance). This explains the broad BESIII width, contrasting with the narrower PDG average. The pattern is consistent with the well-known $\Lambda(1405)$ two-pole scenario, where a higher pole lies close to the real axis and a lower, broader pole appears [31,32,37]. We note that previous chiral unitary approach calculations (e.g., Ref. [29]), which do not perform a combined fit to the three invariant mass spectra, give a somewhat different two-pole pattern ($1824-31i$ MeV and $1875-130i$ MeV). This difference highlights the sensitivity of the pole pattern to the underlying dynamics and the importance of using high-precision data to constrain theoretical models. Although our dynamical generation picture provides a natural explanation for the two-pole pattern, we do not exclude the possibility that the $\Xi(1820)$ may have a sizeable conventional three-quark component. A quantitative distinction between dynamically generated and elementary baryon states can be investigated through various theoretical approaches, such as the Weinberg compositeness criterion. Further experimental and theoretical studies are needed to discriminate between these scenarios.

In summary, our analysis favors that $\Xi(1690)$ is a virtual state from $\bar{K}\Sigma$ interactions, and $\Xi(1820)$ exhibits a $\Lambda(1405)$-like two-pole structure, reinforcing the dynamical generation of strange baryon resonances.

Acknowledgement

This work was supported by the National Natural Science Foundation of China (Grant No. 12475080).

References

[1] Navas S, Amsler C, Gutsche T *et al.* (Particle Data Group) 2024 *Phys. Rev. D* **110** 030001
[2] Dalitz R H and Tuan S F 1960 *Annals Phys.* **10** 307
[3] Hyodo T and Jido D 2012 *Prog. Part. Nucl. Phys.* **67** 55
[4] Oset E and Ramos A 1998 *Nucl. Phys. A* **635** 99
[5] Hall J M M, Kamleh W, Leinweber D B, Menadue B J, Owen B J, Thomas A W, and Young R D 2015 *Phys. Rev. Lett.* **114** 132002
[6] Nakano T, Ahn D S, Ahn J K *et al.* (LEPS) 2003 *Phys. Rev. Lett.* **91** 012002
[7] Wu J J, Molina R, Oset E, and Zou B S 2010 *Phys. Rev. Lett.* **105** 232001
[8] Yang Z C, Sun Z F, He J, Liu X, and Zhu S L 2012 *Chin. Phys. C* **36** 6
[9] Aaij R, Adeva B, Adinolfi M *et al.* (LHCb) 2015 *Phys. Rev. Lett.* **115** 072001
[10] Aaij R, Abellán Beteta C, Adeva B *et al.* (LHCb) 2019 *Phys. Rev. Lett.*

122 222001
[11] Wu J J, Dulat S, and Zou B S 2009 *Phys. Rev. D* **80** 017503
[12] Wang E, Geng L S, Wu J J, Xie J J, and Zou B S 2024 *Chin. Phys. Lett.* **41** 101401
[13] He J 2025 *Phys. Rev. C* **112** 015205
[14] Gay J B, Armenteros R, Berge J P *et al*. (Amsterdam-CERN-Nijmegen-Oxford) 1976 *Phys. Lett. B* **62** 477
[15] Teodoro D, Diaz J, Dionisi C *et al*. 1978 *Phys. Lett. B* **77** 451
[16] Biagi S F, Bourquin M, Brown R M *et al*. 1987 *Z. Phys. C* **34** 175
[17] Aubert B, Bona M, Karyotakis Y *et al*. (BaBar) 2008 *Phys. Rev. D* **78** 034008
[18] Sumihama M, Adachi I, Ahn J K *et al*. (Belle) 2019 *Phys. Rev. Lett.* **122** 072501
[19] Ablikim M, Achasov M N, Ai X C *et al*. (BESIII) 2015 *Phys. Rev. D* **91** 092006
[20] Ablikim M, Achasov M N, Adlarson P *et al*. (BESIII) 2024 *Phys. Rev. D* **109** 072008
[21] Capstick S and Isgur N 1986 *Phys. Rev. D* **34** 2809
[22] Glozman L Y and Riska D O 1996 *Phys. Rept.* **268** 263
[23] Ramos A, Oset E, and Bennhold C 2002 *Phys. Rev. Lett.* **89** 252001
[24] Sarkar S, Oset E, and Vicente Vacas M J 2005 *Nucl. Phys. A* **750** 294
[25] Khemchandani K P, Marttínez Torres A, Hosaka A, Nagahiro H, Navarra F S, and Nielsen M 2018 *Phys. Rev. D* **97** 034005
[26] Sekihara T 2015 *PTEP* **2015** 091D01
[27] Feijoo A, Valcarce Cadenas V, and Magas V K 2023 *Phys. Lett. B* **841** 137927
[28] Kolomeitsev E E and Lutz M F M 2004 *Phys. Lett. B* **585** 243
[29] Molina R, Liang W H, Xiao C W, Sun Z F, and Oset E 2024 *Phys. Lett. B* **856** 138872
[30] Liang W H, Molina R, and Oset E 2024 *Phys. Rev. D* **110** 036005
[31] Oller J A and Meißner U G 2001 *Phys. Lett. B* **500** 263
[32] Jido D, Oller J A, Oset E, Ramos A, and Meißner U G 2003 *Nucl. Phys. A* **725** 181
[33] Albaladejo M, Fernandez-Soler P, Guo F K, and Nieves J 2017 *Phys. Lett. B* **767** 465
[34] Guo F K, Hanhart C, Meißner U G, Wang Q, Zhao Q, and Zou B S 2018 *Rev. Mod. Phys.* **90** 015004
[35] Roca L, Oset E, and Singh J 2005 *Phys. Rev. D* **72** 014002
[36] Geng L S, Oset E, Roca L, and Oller J A 2007 *Phys. Rev. D* **75** 014017
[37] He J and Lu P L 2015 *Int. J. Mod. Phys. E* **24** 1550088
[38] Meißner U G 2020 *Symmetry* **12** 981
[39] Bando M, Kugo T, Uehara S, Yamawaki K, and Yanagida T 1985 *Phys. Rev. Lett.* **54** 1215
[40] Birse M C 1996 *Z. Phys. A* **355** 231
[41] de Swart J J 1963 *Rev. Mod. Phys.* **35** 916
[42] Ronchen D, Doring M, Huang F, Haberzettl H, Haidenbauer J, Hanhart C, Krewald S, Meißner U G, and Nakayama K 2013 *Eur. Phys. J. A* **49** 44
[43] Janssen G, Holinde K, and Speth J 1996 *Phys. Rev. C* **54** 2218
[44] Oh Y, Nakayama K, and Lee T S H 2006 *Phys. Rept.* **423** 49
[45] Matsuyama A, Sato T, and Lee T S H 2007 *Phys. Rept.* **439** 193
[46] Lenske H and DharMand Gaitanos T 2016 arXiv: 1602.08917[nucl-th]
[47] He J and Chen D Y 2019 *Eur. Phys. J. C* **79** 887
[48] He J 2014 *Phys. Rev. D* **90** 076008
[49] He J 2015 *Phys. Rev. D* **92** 034004
[50] He J and Chen D Y 2018 *Eur. Phys. J. C* **78** 94
[51] He J 2015 *Phys. Rev. C* **91** 018201
[52] He J 2016 *Phys. Lett. B* **753** 547
[53] Duan M Y, Song J, Liang W H, and Oset E 2024 *Eur. Phys. J. C* **84** 947
[54] James F E 1968 *Monte-Carlo phase space* CERN-68-15
[55] https://github.com/junhe1979/DalitzPlot.jl